https://dx.doi.org/10.1364/OL.386429

Coherent mid-infrared supercontinuum generation in tapered suspended-core $As_{39}Se_{61}$ fibers pumped by a few-optical-cycle Cr:ZnSe laser

STANISLAV O. LEONOV,[1] YUCHEN WANG,[2] VLADIMIR S. SHIRYAEV,[3] GENNADY E. SNOPATIN,[3] BORIS S. STEPANOV,[3] VICTOR G. PLOTNICHENKO,[4] EDOARDO VICENTINI,[2,5] ALESSIO GAMBETTA,[2,5] NICOLA COLUCCELLI,[2,5] CESARE SVELTO,[6] PAOLO LAPORTA,[2,5] AND GIANLUCA GALZERANO[2,5,*]

[1]*Bauman Moscow State Technical University, 2nd Baumanskay St. 5/1, 105005 Moscow, Russia*
[2]*Istituto di Fotonica e Nanotecnologie – CNR, Piazza Leonardo da Vinci 32, 20133 Milano, Italy*
[3]*G.G. Devyatykh Institute of Chemistry of High-Purity Substances of the Russian Academy of Sciences, 49 Tropinin Str., 603951 Nizhny Novgorod, Russia*
[4]*Fiber Optics Research Center of the Russian Academy of Sciences, 38 Vavilov Str., 119333 Moscow, Russia*
[5]*Dipartimento di Fisica—Politecnico di Milano, Piazza Leonardo da Vinci 32, 20133 Milano, Italy*
[6]*Dipartimento di Elettronica e Informazione e Bioingegneria, Politecnico di Milano, Milan, Italy*
**Corresponding author: gianluca.galzerano@polimi.it*

We report on efficient supercontinuum generation in tapered suspended-core $As_{39}Se_{61}$ fibers pumped by a femtosecond mode-locked Cr:ZnSe laser. The supercontinuum spectrum spans the mid-infrared spectral region from 1.4 to 4.2 μm, and its spectral coherence is proved by heterodyning with a single-frequency narrow-linewidth Er-fiber laser at 1.55 μm, measuring a beat note with 27-dB signal-to-noise ratio in a resolution bandwidth of 100 kHz. The intensity stability of the supercontinuum radiation is also characterized by relative intensity noise measurements.

https://doi.org/10.1364/OL.386429

A wide number of applications in medical diagnostics, environmental and physical sciences, industry, and homeland security has propelled the development of middle-infrared (mid-IR) spectroscopic systems for sensitive and rapid multispecies molecular analysis in the wavelength range from 2 to 5 μm. Frequency-comb-based spectroscopic systems [1] have been shown to offer an extremely promising solution, since they are inherently broadband, they can take advantage of high-finesse optical cavities to enhance sensitivity [2], and, in addition, they lend themselves to the adoption of extremely fast detection systems based on a dual-comb approach [3]. In the last decade, many efforts have been made to demonstrate mid-IR frequency comb synthesizers [4], either starting from near-IR sources and using nonlinear parametric down conversion methods, such as difference frequency generation (DFG) [5], the optical parametric oscillator (OPO) [6], and four-wave mixing interaction in micro-resonators [7], or using quantum cascade (QCL) [8] and interband cascade (ICL) [9] laser combs. Each of these solutions presents some limitations or weaknesses. Most nonlinear methods, in fact, are characterized by complex experimental setups (optical amplifiers and multiple frequency stabilization loops), whereas QCL combs show a relatively narrow spectral bandwidth (~ 10% of the carrier frequency). An interesting technological solution to synthesize a mid-IR comb is based on the femtosecond mode-locked Cr:ZnSe laser [10], the mid-IR analogy of the Ti:sapphire laser, which, in principle, can demonstrate either better performance (wider bandwidth) with respect to QCL/ICL combs or simpler sets compared to OPO/DFG combs. The synthesis of self-referenced optical frequency combs needs efficient generation of a coherent supercontinuum (SC) radiation covering at least one octave, to enable the detection and control of the comb offset frequency by the so-called f-2f interferometer [11]. In the mid-IR spectral region, a promising root for SC generation is given by nonlinear optical fibers based on soft glasses such as fluoride, chalcogenide, and tellurite. Among different glass compositions, chalcogenides have the highest nonlinearity [12,13] and thus can be efficiently exploited with high-repetition-rate femtosecond pulses. Several high-repetition-rate SC generations (~ 80 MHz) have been demonstrated using microstructured chalcogenide fibers pumped at different wavelengths in the range from 1.8 to 4 μm, such as a three-hole As_2S_3 fiber demonstrating SC from 1.2 to 3.2 μm [14] and from 0.6 to 4.1 μm [15], an $As_2Se_3 - As_2S_3$ hybrid four-hole fiber (SC from 1.25 to 5.4 μm) [16], and a tapered suspended-core As_2S_3 fiber (SC from 2.2 to 5.5 μm) [17]. Yet, a comprehensive characterization of the coherence

properties of these SC spectra has not been so far reported. Even a much broader mid-IR SC, spanning from 1.5 to ~ 16 μm, has been demonstrated pumping different types of chalcogenide fibers with low-repetition-rate (~ 1 kHz) and high-energy pulses (μJ) [18–22], which are, however, unsuitable for the synthesis of frequency comb sources.

In this Letter, we report on SC generation covering the mid-IR spectral region from 1.4 to 4.2 μm in tapered suspended-core $As_{39}Se_{61}$ fibers (SCFs) pumped by an ultrafast Cr:ZnSe laser, generating 38-fs pulse trains at 2.4 μm with 170-MHz repetition frequency. A maximum SC average power of ~ 35 mW is obtained for an input average power of 90 mW, demonstrating an optical efficiency of ~ 35%. The spectral coherence of the generated SC is proved by heterodyning it with a single-frequency narrow-linewidth Er-fiber laser at 1.55 μm and by measuring the relative intensity noise spectrum of the SC at the shortest emission wavelength. The heterodyne beat note is characterized by a signal-to-noise ratio of 27 dB in a resolution bandwidth of 100 kHz, whereas the relative intensity noise of the SC is limited mainly by the noise of the pump Cr:ZnSe laser up to the Fourier frequency region of 100 kHz reaching a white noise floor at −116 dB/Hz for frequencies larger than 300 kHz. With respect to the recent results obtained using femtosecond Cr:ZnS lasers with repetition frequencies in the range from 69 to 90 MHz to pump As_2S_3-silica double-nanospike waveguides [23], step-index fluoride fibers [24], and a silicon nitride (Si_3N_4) waveguide [25], we achieved coherent SC radiation with an equivalent spectral coverage using a more compact laser source with a higher pulse repetition frequency of 170 MHz. Our approach, which does not use any optical amplification stage, is also definitely simpler and more straightforward with respect to that adopted in the recent demonstration of a Cr:ZnS frequency comb in the wavelength region from 1.79 to 2.86 μm [26].

To fabricate the SCFs, the sample of high-purity arsenic selenide glass was prepared by melting the initial elements, 6 N purity As and 5 N purity Se, in an evacuated silica-glass ampoule in a rocking furnace using the chemical-distillation method of purification [27]. A target glass composition of $As_{39}Se_{61}$ was selected due to better stability against crystallization compared to $As_{40}Se_{60}$ glass. After distillation and homogenization, the glass composition, examined by energy-dispersive x-ray microanalysis, showed the final stoichiometry $As_{39.0\pm0.2}Se_{61.0\pm0.2}$. From this glass sample, the rod of 16-mm diameter and 100-mm length with parallel-plate polished surfaces was produced. Three longitudinal holes with a diameter of 2.3 mm were drilled in the glass rod using a special high-precision drilling machine. To reduce the surface roughness after drilling, the inner surface of the capillaries was chemically polished with an $H_2SO_4 + 0.015$ mol/l $K_2Cr_2O_7$ solution for 30 min. The preform was drawn into a SCF with an outer diameter of 260 μm [28]. The resulting core diameter and bridge widths were, respectively, 10 μm and 1.5 μm as measured by an optical microscope (ZEISS Axio Imager 2) [see left panel in Fig. 1(a)]. The SCFs were multimode, even for a very thin core diameter of 1 μm, due to the large index mismatch between glass and air [28]. By means of the cut-back technique, 5 dB/m fiber propagation losses were measured at the wavelength of 2.45 μm. Fiber group velocity dispersion in the wavelength range from 1.2 to 1.9 μm was also measured using a homemade setup based on an unbalanced Mach–Zehnder interferometer, where a 90-mm-long test fiber was placed in one arm and an optical delay line in another arm for group delay dispersion

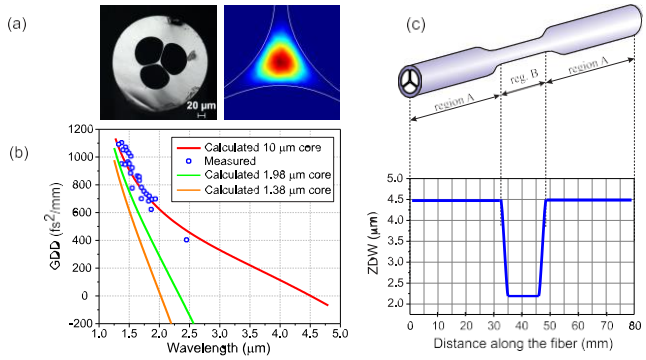

Fig. 1. (a) Cross section of the $As_{39}Se_{61}$ SCF (left image) and computed intensity of the first fiber mode at 2.4 μm (right image). (b) Comparison between the measured and calculated group velocity dispersions. (c) Fiber taper geometry and computed zero-dispersion wavelength along the fiber taper.

(GDD) compensation. Figure 1(b) shows the measured GDD together with the calculated GDD (first mode), using the fiber cross-section geometry and the $As_{39}Se_{61}$ refractive index [29]. Finally, exploiting a homemade setup for standard precision local pulling of fibers [30], a tapering of SCF was performed with two tapered regions of 10-mm and 5-mm length and outer diameters at the taper waist of 65 ± 1 μm and 45 ± 1 μm, respectively. Assuming an adiabatic transition during the tapering, the ratio between core and cladding scaled with the same factor resulting in minimum core diameters of 1.98 μm and 1.38 μm. The calculated zero-dispersion wavelength was therefore shifted from the 4.5-μm un-tapered value to 2.2 μm for the longest tapered fiber [Fig. 1(c)] [28]. As far as the propagation losses are concerned, no particular differences between the un-tapered and tapered fibers were observed being the measured 2.4-μm transmissions at the same level.

Figure 2 shows the experimental setup for SC generation and characterization. A homemade Kerr-lens mode-locked (KLM) Cr:ZnSe laser, based on an asymmetric x-shaped linear resonator similar to that reported in Ref. [31] but with shorter pulse duration, is used as pump source. Optimization of the intracavity GDD is achieved by inserting in the longest resonator arm a 300-μm-thick undoped ZnS plate at Brewster angle. At around 2.4-μm wavelength, the net round-trip intracavity GDD is −110 fs². At 3.2-W pump power, a maximum

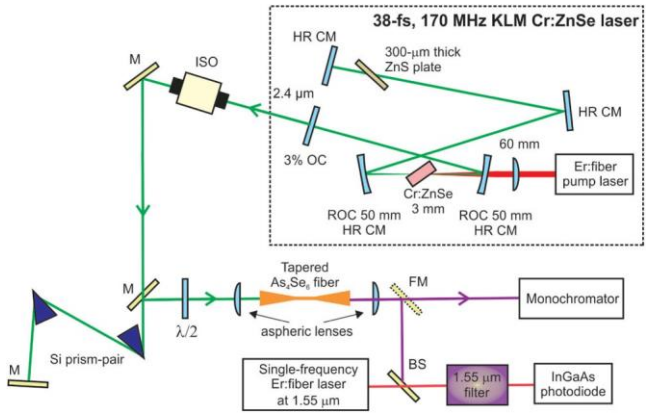

Fig. 2. Experimental setup for SC generation and characterization. BS, beam splitter; HR CM, high-reflectivity chirped mirror; M, gold mirror; FM, flip mirror; ISO, optical isolator.

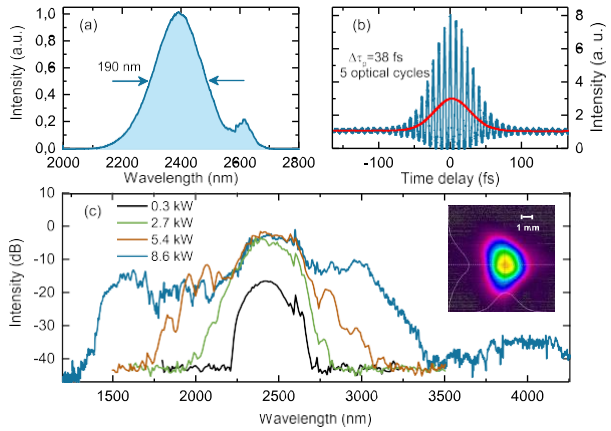

Fig. 3. (a) Optical spectrum and (b) interferometric two-photon autocorrelation of the few-optical-cycle Cr:ZnSe laser. (c) Supercontinuum spectra at different values of the coupled pump peak power for a 10-mm-long tapered SCF sample (inset: far field image of the SC beam).

average output power of ~ 150 mW is obtained for single-pulse mode locking with a pulse repetition frequency of ~ 170 MHz. Figures 3(a) and 3(b) show, respectively, the pulse spectrum and the corresponding interferometric autocorrelation. The emission wavelength is centered at 2390 nm with a full width at half maximum (FWHM) of 190 nm, corresponding to a bandwidth of 9.9 THz. The retrieved pulse duration from interferometric autocorrelation is 38 fs (five optical cycles), corresponding to a time-bandwidth product of 0.38, slightly larger than the transform-limited sech^2 product of 0.32, indicating a small residual pulse chirp. A preliminary characterization of the GDD of the un-tapered SCF is performed by coupling the ultrashort laser pulses to a 10-cm-long fiber and measuring the pulse duration at the fiber output by interferometric autocorrelation. The GDD value is +400 fs^2/mm, in good agreement with the calculated GDD, as shown in Fig. 1(b). Subsequently, the Cr:ZnSe pulse train, pre-chirped in dispersion by a pair of Si prisms (tip-to-tip distance variable in the range from 15 to 35 cm) to achieve the shortest pulse duration in the tapered region, is coupled to the tapered SCF samples through a 1.8-mm mid-IR aspheric lens (AR-coated for 1.5–3 μm). The fiber output beam is collimated by an uncoated 20-mm plano-convex CaF_2 lens and is then analyzed by using a mid-IR monochromator. For both 5-mm- and 10-mm-long tapers, the SC spectra are optimized in bandwidth by changing the prism tip-to-tip separation and rotating the input linear polarization axis by a half-wave plate. The broadest SC spectra are obtained using the 10-mm-long taper. Figure 3(c) shows the SC spectra for the 10-mm tapered fiber at different input peak power levels. The broadest SC generation is obtained at the maximum peak pump power level of 15 kW (corresponding to an average input power of 95 mW), showing a −20-dB bandwidth larger than one octave from 1.45 to 3.15 μm, and with a relative power level of −35 dB at the longest emission wavelength of 4.2 μm. At this maximum input pump power, a SC average power of 35 mW is measured at the fiber output, which corresponds to an optical-to-optical throughout larger than 35%. Taking into account Fresnel reflections at the air–$As_{39}Se_{61}$ interfaces (21% each) and 0.5-dB propagation losses, a coupling efficiency larger than 65% is estimated. For the shortest 5-mm-long taper, the SC spectra are narrower with the same average output power level. In this case, the broadest SC spans from 2.0 to 2.75 μm at −20-dB level (from 1.7 to 3.3 μm at −30-dB level). For both samples, by solving the generalized nonlinear Schrödinger equation in the frequency domain [32], the SC spectra at the fiber output are calculated, taking into account the dispersion curve reported in Fig. 1(b), Raman effects [33], third-order nonlinearity [12], self-steepening, and shock wave formation [33]. In addition, the spectral coherence of the SC spectrum is numerically simulated by applying random quantum noise (one photon per mode) to the pump pulses and estimating the module of the complex degree of first-order coherence: $|ir^{(1)}(\lambda)| = |\frac{\langle E_1^*(\lambda)E_2(\lambda)\rangle}{\langle|E_1(\lambda)|^2\rangle^{1/2}\langle|E_2(\lambda)|^2\rangle^{1/2}}|$, where $E_1(\lambda)$ and $E_2(\lambda)$ are the complex spectral envelopes of independently generated SC pairs, and the brackets denote the ensemble average [34]. Figure 4(a) summarizes the computations in the case of the broadest SC obtained with the 10-mm tapered fiber. The simulated spectrum shows a fairly good agreement with the experimental one, apart from the spectral region above 3.5 μm, probably due to additional fiber propagation losses for wavelengths longer than 2.9 μm in the tapered region of the fiber [35]. In addition, the degree of coherence calculated using 200 SC pairs is fairly close to unity over the entire spectral range [33].

The spectral coherence of the octave spanning spectrum, generated by the 10-mm-long tapered SCF, is experimentally investigated by heterodyning the blue side of the SC spectrum with a single-frequency CW Er-fiber laser emitting at 1.55 μm. The Er-fiber laser has an emission linewidth of ~ 10 kHz for observation times of 100 ms, ensuring negligible frequency noise contribution to the coherence measurements. The SC and CW radiations are combined through a 50% beam splitter and, after spectral filtering at around 1.55 μm with an optical

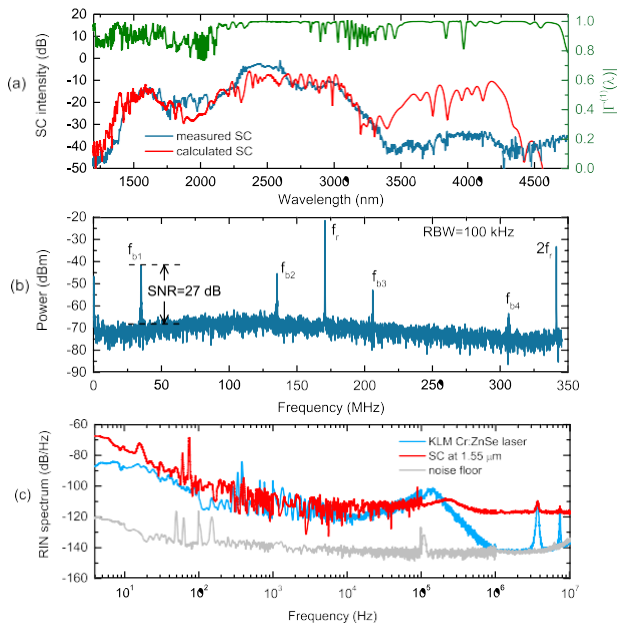

Fig. 4. (a) Computed SC spectrum (red curve) together with the experimental one (blue curve) and first-order coherence as evaluated by 200 SC pairs (green curve) for the 10-mm-long tapered SCF at the maximum peak pump power. (b) Beat note RF spectrum between the SC and the single-frequency narrow-linewidth Er-fiber laser at 1.55 μm. (c) Measured RIN spectrum of the SC at around 1.55 μm (red curve) together with the RIN spectrum of the Cr:ZnSe pump laser (blue curve).

bandwidth of ~ 10 nm (a 2-f optical filter setup constituted by a 600-grooves/mm reflective diffraction grating, a 75-mm focal length plano-convex lens, and a variable slit), the resulting optical field is detected by a fast InGaAs photodetector (see Fig. 2). Figure 4(b) shows the radio-frequency (RF) spectrum of the photocurrent recorded by an electrical spectrum analyzer with resolution bandwidth (RWB) of 100 kHz and spanning frequency range from 0.1 to 340 MHz. Two peaks corresponding to the SC pulse repetition frequency (f_r = 170 MHz) and its second harmonics ($2f_r$ = 340 MHz) are detected together with intermediate peaks due to the beat note signals between the CW and SC radiations (f_{b1}, f_{b2}, f_{b3}, and f_{b4}). The heterodyne signal at the lowest frequency, f_{b1}, corresponding to the beat note between the CW radiation and the closest SC mode, shows a signal-to-noise ratio SNR = 27 dB in 100-kHz RBW, indicating a high degree of coherence for the generated SC [36].

For a comprehensive analysis, the intensity stability of the SC is also characterized by RIN measurements [31]. Figure 4(c) shows the measured RIN spectrum of the SC at around 1.55 μm (optical bandwidth ~ 10 nm FWHM) together with the RIN spectrum of the pump KLM Cr:ZnSe laser. For Fourier frequencies in the range from 400 to 100 kHz, the SC intensity noise is equivalent to the pump noise, whereas in both the low-frequency (f < 400 Hz) and high-frequency (f > 300 kHz) ranges, some degradation of the SC noise is observed. The low frequency excess noise is ascribed to mechanical perturbations (vibrations) of the coupling optics [34]. The broadband white noise floor behavior in the high-frequency region, at a level of −116 dB/Hz, agrees well with the nonlinear amplification of the input-pulse shot noise [37]. The resulting integrated noise of SC radiation at around 1.55 μm, from 10 MHz down to 4 Hz, amounts to 0.5%, to be compared with the 0.3% instability level of the KLM Cr:ZnSe pump laser. This result indicates that the SC generation in SCFs does not significantly degrade the stability performance of the femtosecond pump source.

In conclusion, we reported on coherent and low-noise SC generation in the mid-IR spectral region from 1.4 to 4.2 μm in tapered SCFs pumped by a low-energy few-optical-cycle KLM Cr:ZnSe laser at 2.4 μm. The high degree of the SC spectral coherence and the low excess noise with respect to pump Cr:ZnSe laser paves the way for the implementation of a mid-IR optical frequency comb synthesizer based on low-energy, high-repetition-frequency Cr:ZnSe laser technology and tapered chalcogenide suspended-core fiber.

Funding. Russian Foundation for Basic Research (17-08-00495); Ministero dell'Istruzione, dell'Università e della Ricerca (ESFRI Roadmap - ELI); Regione Lombardia (n.19363/RCC Cybersort).

Disclosures. The authors declare no conflicts of interest.

REFERENCES

1. N. Picqué and T. W. Hänsch, Nat. Photonics **13**, 146 (2019).
2. M. J. Thorpe and J. Ye, Appl. Phys. B **91**, 397 (2008).
3. F. Keilmann, C. Gohle, and R. Holzwarth, Opt. Lett. **29**, 1542 (2004).
4. A. Schliesser, N. Picqué, and T. W. Hänsch, Nat. Photonics **6**, 440 (2012).
5. S. M. Foreman, A. Marian, J. Ye, E. A. Petrukhin, M. A. Gubin, O. D. Muecke, F. N. C. Wong, R. P. Ippen, and F. X. Kaertner, Opt. Lett. **30**, 570 (2005).
6. M. Vainio and L. Halonen, Phys. Chem. Chem. Phys. **18**, 4266 (2016).
7. T. J. Kippenberg, R. Holzwarth, and S. A. Diddams, Science **332**, 555 (2011).
8. A. Hugi, G. Villares, S. Blaser, H. C. Liu, and J. Faist, Nature **492**, 229 (2012).
9. M. Bagheri, C. Frez, L. A. Sterczewski, I. Gruidin, M. Fradet, I. Vurgaftman, C. L. Canedy, W. W. Bewley, C. D. Merritt, C. S. Kim, M. Kim, and J. R. Meyer, Sci. Rep. **8**, 3322 (2018).
10. S. Mirov, I. Moskalev, S. Vasilyev, V. Smolski, V. Fedorov, D. Martyshkin, J. Peppers, M. Mirov, A. Dergachev, and V. Gapontsev, IEEE J. Sel. Top. Quantum Electron. **24**, 1 (2018).
11. D. J. Jones, S. A. Diddams, J. K. Ranka, A. Stentz, R. S. Windeler, J. L. Hall, and S. T. Cundiff, Science **288**, 635 (2000).
12. A. Zakery and S. R. Elliott, J. Non-Cryst. Solids **330**, 1 (2003).
13. G. E. Snopatin, V. S. Shiryaev, G. E. Plotnichenko, E. M. Dianov, and M. F. Churbanov, Inorg. Mater. **45**, 1439 (2009).
14. I. Savelii, O. Mouawad, J. Fatome, B. Kibler, F. Desevedavy, G. Gadret, J. C. Jules, P. Y. Bony, H. Kawashima, W. Gao, T. Kohoutek, T. Suzuki, Y. Ohishi, and F. Smektala, Opt. Express **20**, 27083 (2012).
15. O. Mouawad, J. Picot-Clémente, F. Amrani, C. Strutynski, J. Fatome, B. Kibler, F. Désévédavy, G. Gadret, J.-C. Jules, D. Deng, Y. Ohishi, and F. Smektala, Opt. Lett. **39**, 2684 (2014).
16. T. Cheng, Y. Kanou, X. Xue, D. Deng, M. Matsumoto, T. Misumi, T. Suzuki, and Y. Ohishi, Opt. Express **22**, 23019 (2014).
17. A. Marandi, C. W. Rudy, V. G. Plotnichenko, E. M. Dianov, K. L. Vodopyanov, and R. L. Byer, Opt. Express **20**, 24218 (2012).
18. Z. Zhao, B. Wu, X. Wang, Z. Pan, Z. Liu, P. Zhang, X. Shen, Q. Nie, S. Dai, and R. Wang, Laser Photon. Rev. **11**, 1700005 (2017).
19. T. Cheng, K. Nagasaka, T. H. Tuan, X. Xue, M. Matsumoto, H. Tezuka, T. Suzuki, and Y. Ohishi, Opt. Lett. **41**, 2117 (2016).
20. C. R. Petersen, U. Møller, I. Kubat, B. Zhou, S. Dupont, J. Ramsay, T. Benson, S. Sujecki, N. Abdel-Moneim, Z. Tang, D. Furniss, A. Seddon, and O. Bang, Nat. Photonics **8**, 830 (2014).
21. H. Ou, S. Dai, P. Zhang, Z. Liu, X. Wang, F. Chen, H. Xu, B. Luo, Y. Huang, and R. Wang, Opt. Lett. **41**, 3201 (2016).
22. Z. Zhao, X. Wang, S. Dai, Z. Pan, S. Liu, L. Sun, P. Zhang, Z. Liu, Q. Nie, X. Shen, and R. Wang, Opt. Lett. **41**, 5222 (2016).
23. S. Xie, N. Tolstik, J. C. Travers, E. Sorokin, C. Caillaud, J. Troles, P. St.J. Russell, and I. T. Sorokina, Opt. Express **24**, 12406 (2016).
24. N. Nagl, K. F. Mak, Q. Wang, V. Pervak, F. Krausz, and O. Pronin, Opt. Lett. **44**, 2390 (2019).
25. D. Martyshkin, V. Fedorov, T. Kesterson, S. Vasilyev, H. Guo, J. Liu, W. Weng, K. Vodopyanov, T. J. Kippenberg, and S. Mirov, Opt. Mater. Express **9**, 2553 (2019).
26. S. Vasilyev, V. Smolski, J. Peppers, I. Moskalev, M. Mirov, Y. Barnakov, S. Mirov, and V. Gapontsev, Opt. Express **27**, 35079 (2019).
27. V. S. Shiryaev and M. F. Churbanov, J. Non-Cryst. Solids **475**, 1 (2017).
28. E. A. Anashkina, V. S. Shiryaev, M. Y. Koptev, B. S. Stepanov, and S. V. Muravyev, J. Non-Cryst. Solids **480**, 43 (2018).
29. C. Caillaud, C. Gilles, L. Provino, L. Brilland, T. Jouan, S. Ferre, M. Carras, M. Brun, D. Mechin, J.-L. Adam, and J. Troles, Opt. Express **24**, 7977 (2016).
30. A. P. Velmuzhov, M. V. Sukhanov, T. V. Kotereva, N. S. Zernova, V. S. Shiryaev, E. V. Karaksina, B. S. Stepanov, and M. F. Churbanov, J. Non-Cryst. Solids **517**, 70 (2019).
31. Y. Wang, T. T. Fernandez, N. Coluccelli, A. Gambetta, P. Laporta, and G. Galzerano, Opt. Express **25**, 25193 (2017).
32. J. C. Travers, M. H. Frosz, and J. M. Dudley, *Supercontinuum Generation in Optical Fibers* (Cambridge University, 2010).
33. L. Liu, K. Nagasaka, G. Qin, T. Suzuki, and Y. Ohishi, Appl. Phys. Lett. **108**, 011101 (2016).
34. J. M. Dudley and S. Coen, Opt. Lett. **27**, 1180 (2002).
35. C. R. Petersen, R. D. Engelsholm, C. Markos, L. Brilland, C. Caillaud, J. Trolès, and O. Bang, Opt. Express **25**, 15336 (2017).
36. T. W. Neely, T. A. Johnson, and S. A. Diddams, Opt. Lett. **36**, 4020 (2011).
37. K. L. Corwin, N. R. Newbury, J. M. Dudley, S. Coen, S. A. Diddams, K. Weber, and R. S. Windeler, Phys. Rev. Lett. **90**, 113904 (2003).